Tellus (1996), 48A, 1–16
Printed in Belgium – all rights reserved

TELLUS
ISSN 0280–6495

Annual variation of the global precipitable water and its maintenance: observation and climate-simulation

By TSING-CHANG CHEN* and MING-CHENG YEN, *Department of Geological and Atmospheric Sciences, Iowa State University, Ames, IA 50011, USA*; JAMES PFAENDTNER and Y. C. SUD, *Laboratory for Atmospheres, NASA/Goddard Space Flight Center, Greenbelt, Maryland, 20771, USA*

(Manuscript received 5 April 1994; in final form 21 March 1995)

ABSTRACT

The annual variation of the global-mean precipitable water $\langle W \rangle$ and the associated hydrological cycle were analyzed with the upper-air data generated by the Global Data Assimilation System of the National Meteorological Center for 1981–1991 and the European Centre for Medium Range Weather Forecasts from 1983–1991. It was found that the annual variation of $\langle W \rangle$ coincides with that of the Northern Hemisphere precipitable water $[W]_{NH}$. The hemispheric-mean ($[\ ]$) water budget analysis shows that water vapor is transported from the winter to the summer hemisphere across the equator by the Hadley circulation, and that the annual variations in the water vapor sink $[P-E]$ for both hemispheres also follow the same seasonal march. The amplitudes of the annual variations in these two hydrological processes are comparable in both hemispheres. Thus, the annual variations of $[W]_{NH}$ and $[W]_{SH}$ are the result of slight imbalances between the cross-equator water vapor transport and the water vapor sink, particularly in the spring and fall. The climatological hemispheric-mean water budgets reveal that the Southern Hemisphere is a water vapor source and the Northern Hemisphere is a water vapor sink. The cross-equator water vapor transport constitutes a major source acting to maintain $[W]_{NH}$, and in turn $\langle W \rangle$. The hydrological mechanism maintaining the observed $\langle W \rangle$ annual variation is consistent with that obtained from the hydrological cycle in a 10-year (1979–1988) climate simulation done at the Goddard Laboratory for Atmospheres as part of their participation in the Atmospheric Model Intercomparison Project (AMIP).

1. Introduction

Being a principal medium for energy transport and exchange, water vapor provides the link connecting various processes of the global hydrological cycle. Although it constitutes only a small portion of the total water contained in the land-ocean-atmosphere system, the atmospheric water vapor plays a vital role in the energy balance of the global climate system. Thus, in addition to its long-term mean climate, we also need to understand the cause and maintenance of the water vapor's low-frequency variability, which is closely related to the low-frequency variability of the global climate. As revealed from Figs. 1 and 2 based on the data generated by the global data assimilation system (GDAS), the global-mean precipitable water exhibits a pronounced annual variation which follows its seasonal cycle in the Northern Hemisphere. Regardless of the numerous efforts made in the past several decades to explore the atmospheric branch of the global hydrological cycle, the annual variation of global precipitable water has not been fully analyzed and understood.

According to the water budget equation, the rate of change of global water vapor is simply equal to evaporation minus precipitation. However, the lack of uniform high quality observations over the globe for precipitation and evaporation does not allow one to determine the rate of change

* Corresponding author.

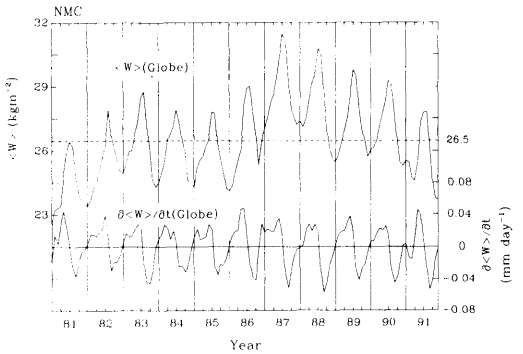

Fig. 1. Annual variations of the global-mean precipitable water $\langle W \rangle$ (the top curve with a multiple-year (1981–1991) mean value of 26.5 kg m^{-2}) and the time rate of change of $\langle W \rangle$, $\partial \langle W \rangle / \partial t$, computed from the NMC GDAS data.

of atmospheric water vapor from observations. Recently, an ambitious plan, the Global Precipitation Science Plan (1992), was initiated by the NOAA Climate and Global Change Program to collect the needed global precipitation data. Even if this plan is successfully pursued, we will still lack the needed quality global evaporation data. In view of the difficulties in collecting global hydrological data and the importance of precipitable water to the global hydrological cycle, an alternative path to improving our understanding of the cause and maintenance of low-frequency variability in the global precipitable water is to analyze the hydrological cycle simulated by a sophisticated full-physics general circulation model (GCM).

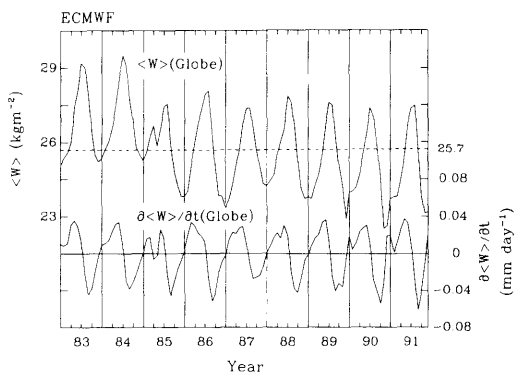

Fig. 2. Same as Fig. 1, except from the ECMWF GDAS data for 1983–1991.

In this study, we shall use the data generated by the GDAS of the National Meteorological Center (NMC) and the European Centre for Medium Range Weather Forecasts (ECMWF) to analyze characteristics of the annual variation of global precipitable water and to establish hypothesis for the cause of this low-frequency variability. The observational data sources are: the 10-level NMC (1981–1991) and the ECMWF (1983–1991) GDAS data with a resolution of 2.5° (longitude) × 2.5° (latitude). A small amount of missing data in the time series were filled by linear interpretation in time. Since the global precipitation and evaporation data are not available, we use the hydrological cycle simulated by the full-physics general circulation model (GCM) of the Goddard Laboratory for Atmospheres (GLA) to substantiate the proposed hypothesis. The GLA GCM developed by Sud and Walker (1993) was integrated to produce a 10-year (1979–1988) climate simulation with externally prescribed sea surface temperatures. The hydrological cycle of this climate simulation will be used to explain the cause and maintenance of annual variations of the global precipitable water.

2. Analysis of assimilated data

The vertically-integrated water budget equation is

$$\frac{\partial W}{\partial t} + \nabla \cdot Q = E - P, \tag{1}$$

where $W = (1/g) \int_0^{p_0} q \, dp$ is the precipitable water of the atmosphere, $Q = (1/g) \int_0^{p_0} (Vq) \, dp$ is the horizontal flux of water vapor, and q, V, p_0, E and P are specific humidity, horizontal velocity, surface pressure, evaporation and precipitation, respectively. Integrating eq. (1) over the globe, the global-mean ($\langle \; \rangle$) water budget equation becomes

$$\frac{\partial \langle W \rangle}{\partial t} = \langle E - P \rangle. \tag{2}$$

Apparently, any variation in the global-mean precipitable water results from an imbalance between global-mean evaporation and precipitation.

The global-mean precipitable water $\langle W \rangle$ computed with the NMC (Fig. 1) and ECMWF (Fig. 2) GDAS data exhibits a pronounced annual variation which is close to those obtained by previous studies (Rosen et al., 1979; Peixoto and Oort, 1983, and others). Some interannual variation of $\langle W \rangle$ due to changes in the two assimilation systems are discernible. The climatological-mean values of $\langle W \rangle$ are slightly different in the two data sets. The annual maximum of $\langle W \rangle$ appears in the northern summer, and its minimum in the northern winter. The $\langle W \rangle$ annual variation is in phase with the annual variation of the Northern Hemispheric mean precipitable water $[W]_{NH}$ (discussed later in this section). As expected, the tendency of global-mean precipitable water $\partial \langle W \rangle / \partial t$ and the deviation of $\langle W \rangle$ from its long-term mean are temporally in quadrature, with $\partial \langle W \rangle / \partial t$ reaching its maximum and minimum values during the Northern Hemisphere spring buildup and fall decline of $\langle W \rangle$, respectively. According to eq. (2), the annual variation of global-mean evaporation minus precipitation ($\langle E-P \rangle$) follows that of $\partial \langle W \rangle / \partial t$. Consistent with the time series of $\partial \langle W \rangle / \partial t$, (Figs. 1, 2), the maximum and minimum values of $\langle E-P \rangle$ occur in northern spring and fall, respectively. As shown in previous studies (Peixoto and Oort, 1983) the hemispheric-mean $E-P$ over the Northern Hemisphere, $[E-P]_{NH}$, attains its maximum and minimum values in the northern winter and summer, respectively. In other words, the annual cycles of $[W]_{NH}$ and $[E-P]_{NH}$ are synchronized. In contrast, annual variations of $\langle W \rangle$ and $\langle E-P \rangle$ are temporally in quadrature. Why should annual variations of the global- and hemispheric-mean water budgets differ in this way?

In view of the global water budget analysis presented above, the following questions are raised.

(1) Why does the annual variation of $\langle W \rangle$ follow the seasonal march of the Northern Hemisphere average $[W]_{NH}$?

(2) Following eq. (2), we expect the annual variations of $\langle E-P \rangle$ and $\langle W \rangle$ to be temporally in quadrature. Why are the annual variations of $\langle E-P \rangle$ and $[E-P]_{NH}$ (or $[E-P]_{SH}$) also temporarilly in quadrature?

(3) It was inferred by Bryan and Oort (1984) and Chen et al. (1995) that the Northern (Southern) Hemisphere is a sink (source) of water vapor. Why does the annual variation of $\langle W \rangle$ follow that of $[W]_{NH}$, instead of $[W]_{SH}$? How do both hemispheres contribute to maintain the global water budget?

In seeking answers to these questions, we need to pursue the hemispheric-mean water budget analysis. The hemispheric-mean water budget equations for the Northern Hemisphere (NH) and the Southern Hemisphere (SH) can be written:

$$\frac{\partial [W]_{NH}}{\partial t} + [\nabla \cdot Q]_{NH} = [E-P]_{NH}, \tag{3}$$

$$\frac{\partial [W]_{SH}}{\partial t} + [\nabla \cdot Q]_{SH} = [E-P]_{SH}. \tag{4}$$

Since $[\nabla \cdot Q]_{NH} + [\nabla \cdot Q]_{SH} = \langle \nabla \cdot Q \rangle = 0$,

$$[\nabla \cdot Q]_{NH} = -[\nabla \cdot Q]_{SH}. \tag{5}$$

Thus, eq. (3) can be written as

$$\frac{\partial [W]_{NH}}{\partial t} - [\nabla \cdot Q]_{SH} = [E-P]_{NH}. \tag{6}$$

Results of the hemispheric-mean water budget analyses from eqs. (4) and (6) with the NMC and ECMWF GDAS data are shown in Figs. 3 and 4, respectively. The $\partial [W]/\partial t$ and $[\nabla \cdot Q]$ terms in eqs. (4) and (6) are computed directly from the two data sets, but $[E-P]_{NH}$ and $[E-P]_{SH}$ are estimated by the residual method through eqs. (4) and (6). Thus, estimates of the two latter quantities may include the computational error and data deficiency. Moreover, the computations of $\partial \langle W \rangle / \partial t$ and $\partial [W]/\partial t$ were made with monthly-mean $\langle W \rangle$ and $[W]$, instead of the available 12-h synoptic data. Consequently, values of $\partial \langle W \rangle / \partial t$ and $\partial [W]/\partial t$ may be underestimated. These underestimations may also result in slight overestimates of $\langle E-P \rangle$ and $[E-P]$. The intensity of the atmospheric hydrological cycle depicted with our analysis is likely to be on the high side. The results, shown in Figs. 3 and 4, will be used to answer the three questions posed earlier.

2.1. *Question 1: Why does the annual variation of $\langle W \rangle$ follow the seasonal march of the Northern Hemisphere average $[W]_{NH}$?*

Chen (1985) and others have shown that atmospheric precipitable water accumulates in the

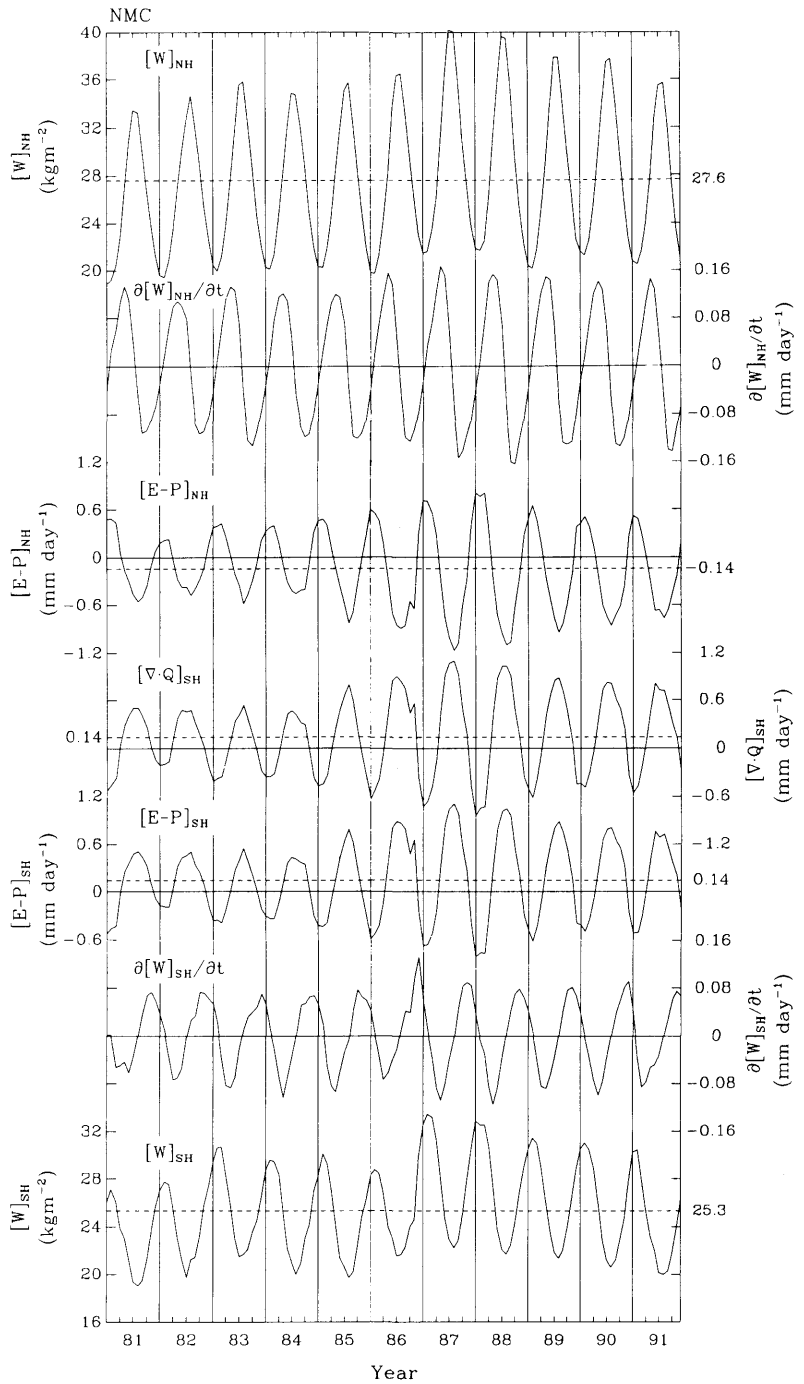

Fig. 3. Annual variations of the hemispheric-mean ([ ]) water budget analysis for both the Northern ($[\ ]_{NH}$) and Southern ($[\ ]_{SH}$) Hemispheres from the NMC GDAS data. Variables included in the analysis are labeled on the individual curves. The horizontal dashed lines shown for several of the variables indicate their multiple-year mean. The mean values are displayed on the right-hand axis.

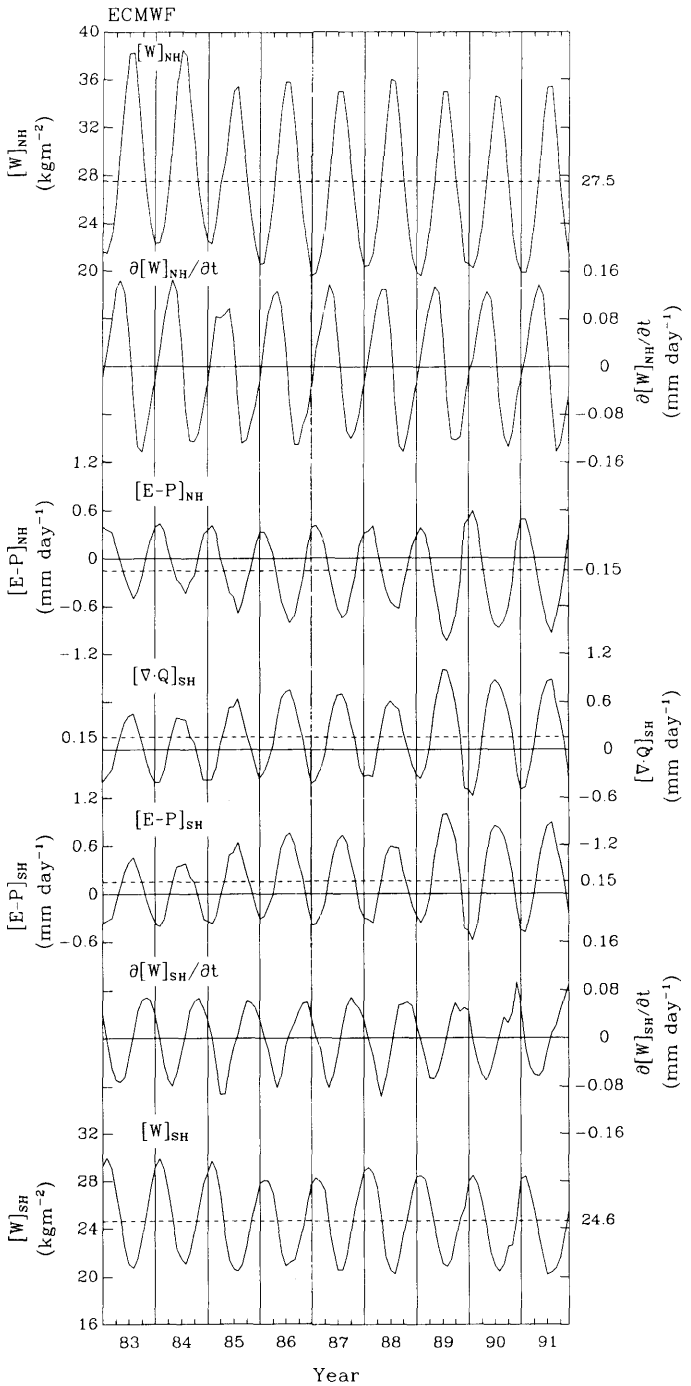

Fig. 4. Same as Fig. 3, except from the ECMWF GDAS data.

Table 1. *Amplitudes and phases of the annual harmonics of various hemispheric-mean hydrological variables computed with the NMC and ECMWF GDAS data and the 10-year simulation with the GLA GCM*

Quantity	NMC	ECMWF	GLA-GCM
$[W]_{NH}$	8.1 (7/19)	7.7 (7/15)	6.8 (7/19)
$[W]_{SH}$	4.8 (1/28)	4.2 (1/27)	3.9 (1/30)
(W)	1.7 (7/3)	1.8 (7/3)	1.8 (7/6)
$\partial[W]_{NH}/\partial t$	0.13 (4/19)	0.13 (4/15)	0.11 (4/20)
$\partial[W]_{SH}/\partial t$	0.08 (10/31)	0.07 (10/28)	0.06 (10/31)
$\partial(W)/\partial t$	0.03 (4/3)	0.03 (4/1)	0.03 (4/18)
$[E-P]_{NH}$	0.7 (7/30)	0.6 (7/27)	0.7 (7/20)
$[E-P]_{SH}$	0.6 (1/23)	0.6 (1/20)	0.8 (1/14)
$(E-P)$	0.03 (4/6)	0.03 (4/16)	0.03 (4/12)
$[\nabla \cdot Q]_{SH}$	0.7 (7/18)	0.6 (7/15)	0.8 (7/12)
$[E-P]_{NH}+[\nabla \cdot Q]_{SH}$			0.11 (3/19)
$[E-P]_{SH}$-$[\nabla \cdot Q]_{SH}$			0.07 (9/26)
$[E-P]_{NH}+[E-P]_{SH}$			0.03 (4/12)

Units of $[W]$ values and various quantities of the water budget equation are kg m^{-2} and mm day^{-1}, respectively. The phase is denoted by the date (month/day) when the annual harmonic attains its maximum value.

tropics. The W-maximum is known to migrate north and south across the equator following the seasonal march of the overhead Sun. Consequently, $[W]_{NH}$ ($[W]_{SH}$) attains its maximum value in the northern summer (winter). As revealed from Figs. 3 and 4, the annual variations of $[W]_{NH}$ (top curves) and $[W]_{SH}$ (bottom curves) vary out of phase. The amplitudes of $[W]_{NH}$ and $[W]_{SH}$ are about 8 and 4 kg m^{-2}, respectively. Because $\langle W \rangle = 1/2([W]_{NH}+[W]_{SH})$ and amplitude ($[W]_{NH}$) > amplitude($[W]_{SH}$), it becomes obvious why the annual variation of $\langle W \rangle$ follows that of $[W]_{NH}$ with an amplitude of approximately 2 kg m^{-2} (Table 1). The contrast between the amplitudes of the annual variations of $[W]_{NH}$ and $[W]_{SH}$ is consistent with Trenberth's (1987) analysis and also answers the first question.

Stephens (1990) found that monthly-mean precipitable water obtained from passive microwave radiometry (SMMR) are correlated with the sea surface temperature (SST). The annual variations of Stephens' area-mean precipitable water over both the Northern- and Southern-Hemisphere oceans are close to the annual variations of our hemispheric-mean values shown in Figs. 3 and 4, except that the phases of Stephens' annual variations are about a month behind ours. It was shown by Chen and Tzeng (1990) that centers of the W annual-cycle mode are located in the three tropical continents. As argued by Stephens, the continents exert a significant effect on the W annual cycle of the globe. However, the one-month phase lag between Stephens' and our annual cycle of precipitable water in each hemisphere may be caused by the thermal inertial of oceans.

2.2. *Question 2: Why are the annual variations of $\langle E-P \rangle$ and $[E-P]_{NH}$ (or $[E-P]_{SH}$) temporarily in quadrature?*

Eqs. (6) and (4) can be written as:

$$\frac{\partial [W]_{NH}}{\partial t} = [E-P]_{NH} + [\nabla \cdot Q]_{SH} \tag{7}$$

and

$$\frac{\partial [W]_{SH}}{\partial t} = [E-P]_{SH} - [\nabla \cdot Q]_{SH}. \tag{8}$$

It has been shown in numerous studies (Oort, 1971) that the Hadley circulation is largely responsible for the interhemispheric exchange of atmospheric mass across the equator from the winter to the summer hemisphere in the lower troposphere and from the latter to the former hemisphere in the upper troposphere. Because water vapor mainly exists in the lower troposphere, it is transported from the winter to the summer hemisphere, namely from the drier to wetter hemisphere as indicated by the annual variations of $[\nabla \cdot Q]_{SH}$ (Figs. 3 and 4).

To supply water vapor for this interhemispheric transport and to maintain the seasonal march of the Hadley circulation described above, the winter (summer) hemisphere should have water vapor surplus (deficit), i.e., $[E-P]>0\ (<0)$. The rationale of this hypothesis is confirmed by Figs. 3 and 4 which show: (a) the annual variations of $[E-P]_{SH}$ and $[\nabla\cdot Q]_{SH}$ are synchronized while the annual variation of $[E-P]_{NH}$ is out of phase with them, and (b) the amplitudes of all three annual variations are comparable (about 0.6 mm day^{-1}, Table 1). These hemispheric-mean water budgets are consistent with Peixoto and Oort's (1983) analysis which was done in terms of the seasonal- and latitudinal-mean distributions of various hydrological variables.

According to (7) and (8), for both hemispheres, the temporal variations in $[W]$ result from imbalances between hemispheric-mean water vapor source $[E-P]$ and the equatorial water vapor flux $[\nabla\cdot Q]_{SH}$. The contrast between $\partial[W]/\partial t$ and $[E-P]$ (or $[\nabla\cdot Q]_{SH}$), as shown in Figs. 3 and 4, reveals that the aforementioned imbalances reach their positive (negative) maximum values in spring (fall). Thus, $[W]$ develops maximum (minimum) values about a season (a quarter of annual cycle) behind $\partial[W]/\partial t$. From the annual variations of the hemispheric-mean water budgets, it is clear that the cross-equator water vapor transport by the Hadley circulation plays a vital role in maintaining annual variations of the hemispheric-mean precipitable water in both hemispheres.

Combining eqs. (6) and (7) gives:

$$\frac{\partial\langle W\rangle}{\partial t}=\frac{1}{2}\left\{\frac{\partial[W]_{NH}}{\partial t}+\frac{\partial[W]_{SH}}{\partial t}\right\}$$

$$=\frac{1}{2}\{[E-P]_{NH}+[E-P]_{SH}\}$$

$$=\langle E-P\rangle. \qquad (9)$$

According to this equation, the annual variation of $\partial\langle W\rangle/\partial t$ can be determined by averaging the annual variations of $\partial[W]_{NH}/\partial t$ and $\partial[W]_{SH}/\partial t$. As shown in Table 1 as well as in Figs. 3 and 4, these two quantities have opposite phases; that is, they have a 6-month phase difference. Thus, the combination of these two annual variations leads to an approximate cancellation. Because the amplitude of $\partial[W]_{NH}/\partial t$ is greater than the amplitude of $\partial[W]_{SH}/\partial t$, the annual variation of $\partial\langle W\rangle/\partial t$ is mainly determined by that of $\partial[W]_{NH}/\partial t$. On the other hand, we may consider the annual variation of $\partial\langle W\rangle/\partial t$ to be the response of the global precipitable water to the combined variations in the water vapor source in the two hemispheres: $[E-P]_{NH}$ and $[E-P]_{SH}$. The composite annual variations of these two quantities are shown in Fig. 5, where the sign of $[E-P]_{NH}$ has been changed to reflect the opposing seasonal marches in the two hemispheres. For each hemisphere, the fall $[E-P]$ is always larger than the corresponding spring $[E-P]$ of the other hemisphere. This difference between $[E-P]$ in the two hemispheres results in the spring maximum (fall minimum) of $\langle E-P\rangle$ $(=\partial\langle W\rangle/\partial t)$, and in turn the spring buildup and the fall reduction of $\langle W\rangle$ shown in Figs. 1 and 2.

Although the budget analysis following eq. (9) answers *Question* 2, the physical mechanism responsible for the occurrence of the spring maximum and fall minimum in $\langle E-P\rangle$ is still unclear. In order to identify the mechanisms, we compare the planetary divergent circulation, and the associated water vapor transport and water vapor source $\langle E-P\rangle$ between late northern spring and early northern fall. Near the end of northern spring, the Sun is well advanced into the Northern Hemisphere and the summer Asian monsoon begins to emerge. As inferred from the region of strong negative $\Delta(E-P)$ $\{=(E-P)_{(\text{May–June})}-(E-P)_{(\text{September–October})}\}$ shown in Figs. 6b and 6d, the upper-level divergence center over the monsoon region (not shown) is intensified and water vapor convergence toward this region, as indicated by $\Delta(\chi_Q, Q_D)$, is enhanced (compared to the early northern fall condition) to maintain the monsoon rain. Simultaneously, the upper-level convergence center outside the monsoon region is also intensified and positive $\Delta(E-P)$ becomes significant along the ITCZ in the eastern Pacific and the Atlantic, and over South Africa. Consequently, these three positive $\Delta(E-P)$ centers make $\langle E-P\rangle$ reach its maximum in the northern spring. At the beginning of the northern fall, the Sun moves across the equator to the Southern Hemisphere and the summer Asian monsoon decays. In this phase, the late northern spring conditions of upper-level divergence and the hydrological processes are reversed: as revealed

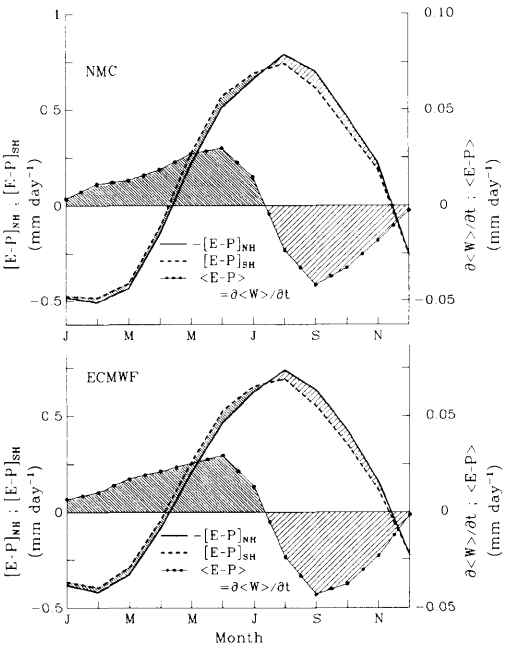

Fig. 5. Composite charts of $-[E-P]_{NH}$ (solid line), $[E-P]_{SH}$ (dashed line) and the sum of these two hydrological variables $\langle E-P\rangle$ (solid-dot line). The positive (negative) values of $\partial\langle W\rangle/\partial t$ and $([E-P]_{SH}+[E-P]_{NH})$ are heavily (lightly) stippled. The top composite chart is constructed with the hemispheric-mean water budget of the NMC GDAS data shown in Fig. 3, while the bottom composite chart is constructed with that of the ECMWF GDAS data shown in Fig. 4.

from $\Delta(\chi_Q, \boldsymbol{Q}_D)$, relatively more water vapor diverges from the Asian monsoon region to the three aforementioned tropical regions to maintain the enhanced precipitation and to make $\Delta(E-P)$ negative in those regions. These negative $\Delta(E-P)$ centers during early northern fall result in a minimum of $\langle E-P\rangle$.

As inferred from the discussion above, the spring maximum and fall minimum $\langle E-P\rangle$ are determined by the seasonal change in $(\chi_Q, \boldsymbol{Q}_D)$ between the two transition seasons, $\Delta(\chi_Q, \boldsymbol{Q}_D)$. However, to fully appreciate this argument, we need to know how significant $\Delta(\chi_Q, \boldsymbol{Q}_D)$ is quantitatively. For this purpose, the spring-mean $(\chi_Q, \boldsymbol{Q}_D, E-P)$ fields of both the NMC and ECMWF GDAS data are presented in Figs. 6a and 6c, respectively. A resemblance exists between the spatial structures of $\Delta(\chi_Q, \boldsymbol{Q}_D)$ and $(\chi_Q, \boldsymbol{Q}_D)$ and indicates that the global divergent water-vapor transport is stronger in spring than fall. Moreover, magnitudes of $\Delta(\chi_Q, \boldsymbol{Q}_D, E-P)$ are about a half of the corresponding spring-mean values. Apparently, the hydrological processes $(\chi_Q, \boldsymbol{Q}_D)$ maintaining the seasonal change in $(E-P)$ is quantitatively significant.

2.3. *Question 3: How do both hemispheres contribute to maintain the global water budget?*

This question may be answered by a combination of two perspectives: the maintenance of the planetary divergent circulation by diabatic heating and the water budget analysis. By combining the continuity and thermodynamic equations, Chen and Yen (1991) formulated a simple diagnostic equation in which velocity potential (χ) was directly linked to diabatic heating $(\dot{Q})$ through the following term:

$$\chi \sim \nabla^{-2}\left\{\frac{\partial}{\partial p}\left(\frac{1}{c_p\sigma}\dot{Q}\right)\right\}, \tag{10}$$

where $\nabla^{-2}(\ )$, p, σ and c_p are inverse Laplacian, pressure, static stability and specific heat at constant pressure, respectively. In the tropics, the major contribution to $\dot{Q}$ is the latent heat released by cumulus convection which may be estimated with $-L(E-P)$, where L is latent heat of condensation. Time series of both $[E-P]_{NH}$ and $[E-P]_{SH}$ shown in Figs. 3 and 4 indicate that a positive latent heat source exists for about 7.5 months in the summer Northern Hemisphere and 4.5 months in the summer Southern Hemisphere. Moreover, the climatological mean $[E-P]_{NH} = -0.14\,\text{mm day}^{-1}$ and $[E-P]_{SH} = 0.14\,\text{mm day}^{-1}$, and the amplitudes of the annual variations for both $[E-P]_{NH}$ and $[E-P]_{SH}$ are about 0.6 mm day^{-1}. It is therefore obvious that the Northern Hemisphere receives more latent heating than the Southern Hemisphere. According to eq. (10), a stronger planetary divergent circulation is maintained by larger latent heating during the northern summer (when the major upper level divergence center is located in the Northern Hemisphere) than during the northern winter (when the major upper level divergence center is located in the Southern Hemisphere). Because the Hadley circulation is a part of the planetary divergent circulation, more water vapor is trans-

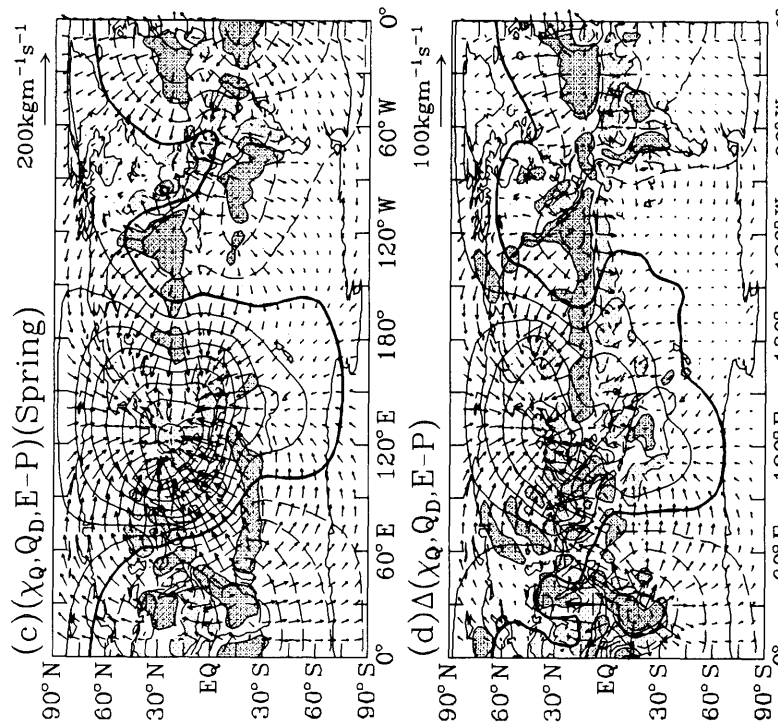

Fig. 6. Composite charts of spring-mean $(\chi_Q, \boldsymbol{Q}_D, E-P)$ (a, c) and $\Delta(\chi_Q, \boldsymbol{Q}_D, E-P)$ $\{=(\chi_Q, \boldsymbol{Q}_D, E-P)_{(\text{May-June})} - (\chi_Q, \boldsymbol{Q}_D, E-P)_{(\text{September-October})}\}$ (b, d). The positive (negative) values of χ_Q and $\Delta\chi_Q$ are contoured with solid (dashed) lines. The contour interval is of χ_Q and $\Delta\chi_Q$ are 4×10^7 kg m^2 s^{-1} and 2×10^7 kg m^2 s^{-1}, respectively. The positive (negative) values of $(E-P)$ and $\Delta(E-P)$ larger (smaller) than 3.0 (-3.0) and 1.5 (-1.5) mm day^{-1}, respectively, are heavily (lightly) shaded. $\boldsymbol{Q}_D$ and $\Delta\boldsymbol{Q}_D$ are represented by vectors with a reference vector shown at the top right of each panel. The left column is prepared with the NMC GDAS data, while the right column with the ECMWF GDAS data.

ported to the Northern from the Southern Hemisphere than vice versa. This inference is substantiated by the time series of $[\nabla \cdot Q]_{SH}$ shown in Figs. 3 and 4. The cross-equator transport of water vapor, $[\nabla \cdot Q]_{SH}$, is northward for about 7.5 months during the northern summer, and southward for about 4.5 months during the northern winter. Like $[E-P]_{NH}$ or $[E-P]_{SH}$, the climatological mean $[\nabla \cdot Q]_{SH}$ is about 0.14 mm day^{-1} and the amplitude of its annual variation is about 0.6 mm day^{-1}. These facts lead us to the conclusion that water vapor is transported across the equator from the water vapor source of the Southern Hemisphere to balance the water vapor sink of the Northern Hemisphere.

So far, our major effort has been to explain the maintenance of the $\langle W \rangle$ annual variation based upon the time variations of the hemispheric-mean hydrological cycle shown in Figs. 3 and 4. However, it may also be informative to examine the overall climatology for the atmospheric branch of the hydrological cycle as summarized in Fig. 7. Because of the lack of quality observations over oceans, the various values of $[E]$ and $[P]$ are not individually computed, and the $[E-P]$ values are estimated by the residual method. In spite of the data deficiency and computational errors, we still obtain a reasonable atmospheric hydrological

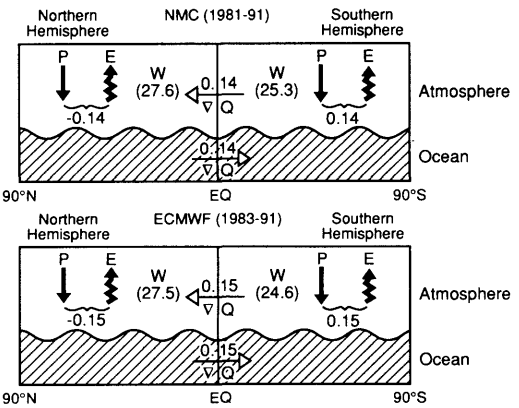

Fig. 7. Schematic diagrams of the hemispheric-mean water budgets analyzed with the NMC (top; 1981–1991) and ECMWF (bottom; 1983–1991) GDAS data; $[P]$ and $[E]$ are denoted with the downward and upward directed vectors, respectively. The numerical values underneath these two vectors are for $[E-P]$. The units for $[W]$ is kg m^{-2}, while those for $[E-P]$ and $[\nabla \cdot Q]$ are mm day^{-1}.

cycle. In order to maintain the hydrological equilibrium of the atmosphere, the cross-equator transport of water vapor $[\nabla \cdot Q]_{SH}$ should be balanced by a return freshwater transport from the Northern to the Southern Hemisphere by the oceans. This return freshwater transport by the oceans shown in Fig. 7 is consistent with previous estimates (Chen et al., 1995) both in direction and magnitude. Finally, regardless of differences between the NMC and ECMWF GDAS, the hemispheric-mean hydrological cycles depicted with the data generated by these two GDASs are close to each other.

3. Climate simulation

The results of the analysis of annual variation of the atmospheric water budget from the NMC and ECMWF GDAS data can be summarized as follows:

(a) The annual variation of $\langle W \rangle$ follows the seasonal variation of $[W]_{NH}$.

(b) The water vapor is transported from the drier atmosphere of the Southern Hemisphere to the wetter atmosphere of the Northern Hemisphere primarily by the Hadley circulation.

(c) The annual variation of $\langle W \rangle$ is a response of the atmospheric hydrological conditions to the annual variation of $\langle E-P \rangle$ which leads the annual variation of $\langle W \rangle$ by 3 months.

However, some deficiencies are known to exist in these GDAS data. First of all, there is no constraint on the moisture field during the GDAS initialization process. This unconstrained treatment of the moisture field could result in some spurious fluctuations in $\langle W \rangle$. The water vapor transport across the equator is driven by the Hadley circulation, and is sensitive to the cumulus scheme used in the GDAS model. Consequently, some significant artificial variations and biases in the Hadley circulation of the GDAS data can be anticipated. Finally, because of the lack of evaporation and precipitation observations, the residual method is used to estimate $\langle E-P \rangle$ through the water budget equation. Thus, the estimation of $\langle E-P \rangle$ is subject to deficiencies of data quality caused by the GDAS biases and the repeated changes made to the GDAS. In view of the possible impacts of poor data quality on con-

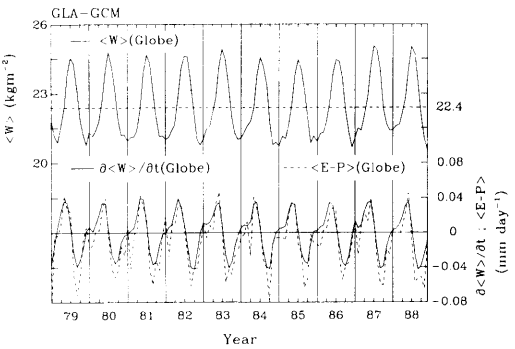

Fig. 8. Same as Fig. 1, except for the global water budget simulated by the GLA GCM. The annual variation of $(E-P)$ (dashed line) is added to the bottom curve $(\partial\langle W\rangle/\partial t)$.

clusions drawn from the water budget analysis with the GDAS data, we need an alternative way of supporting the above conclusions drawn from our analyses using the GDAS data. The best alternative available is to analyze the atmospheric hydrological cycle simulated with a sophisticated full-physics global climate model, although we then need to remember that we are dealing with a simulated and not the real atmosphere. Toward this purpose, we shall analyze a 10-year (1979–1988) climate simulation made with the GLA GCM for the Atmospheric Model Intercomparison Project (AMIP).

The global water budget of the GLA climate simulation is shown in Fig. 8; annual variations of $\langle W\rangle$ (top solid line) with a multiple-year climatological mean value $\langle W\rangle$ ($=22.4\ \mathrm{kg\ m^{-2}}$; straight dashed line) and $\partial(W)/\partial t$ (bottom solid line) superimposed with the annual variation of $\langle E-P\rangle$ (bottom dashed line). The GLA $\langle W\rangle$ is somewhat smaller than those of the NMC ($=26.5\ \mathrm{kg\ m^{-2}}$) and ECMWF ($=25.7\ \mathrm{kg\ m^{-2}}$) analyses. However, those systems use Kuo's cumulus scheme which is known to produce a wetter tropics. As shown in Table 1, the amplitudes of the observed and model $\langle W\rangle$ and $\partial\langle W\rangle/\partial t$ annual variations ($\approx 2\ \mathrm{kg\ m^{-2}}$ and 3×10^{2} mm $\mathrm{day^{-1}}$, respectively) are about equal. The annual variation of the model's $\langle W\rangle$ is coincident with the seasonal march of the Northern Hemisphere as in the GDAS data. According to (1), $\partial\langle W\rangle/\partial t$ is caused by the imbalance between global-mean evaporation and precipitation $\langle E-P\rangle$ which is directly generated by the GLA GCM. As expected, a full correspondence exists between the model's $\partial\langle W\rangle/\partial t$ and $\langle E-P\rangle$, although some minor discrepancies appear which may be attributed to the data interpolation from the σ to pressure coordinates and computational errors. Table 1 shows that the annual variations of the observed and model generated global-mean water budgets are consistent in their amplitudes as well as their phases.

The simulated hemispheric-mean water budgets are shown in Fig. 9. For comparison, amplitudes and phases of the annual harmonics of various hydrological variables are also shown in Table 1. The key findings are as follows.

(a) The amplitudes and phases of the model's $[W]_{\mathrm{NH}}$ and $[W]_{\mathrm{SH}}$ annual harmonics are comparable to the observed. Apparently, the model and observed annual variations of hemispheric-mean precipitable water also are in good agreement with each other. This comparison between the observed and modeled $[W]$ values supports our previous conclusion that the annual variation of global precipitable water is primarily determined by its large variation in the Northern Hemisphere.

(b) The intensity of the model's hemispheric water budgets are revealed through $[E-P]_{\mathrm{NH}}$, $[\nabla\cdot Q]_{\mathrm{SH}}$ and $[E-P]_{\mathrm{SH}}$. The climatological-mean values of these three hydrological variables are about 0.18 mm $\mathrm{day^{-1}}$ which is comparable to the observed. A schematic diagram summarizing the model's climatological-mean hemispheric-mean budgets is presented in Fig. 10 and resembles the observed: water vapor is transported from the drier Southern Hemisphere to the wetter Northern Hemisphere. Amplitudes of the annual variations of $[E-P]_{\mathrm{NH}}$, $[\nabla\cdot Q]_{\mathrm{SH}}$ and $[E-P]_{\mathrm{SH}}$ are about 0.6 mm $\mathrm{day^{-1}}$ and phases of maximum values of $[E-P]_{\mathrm{NH}}$ and the other two hydrological variables fall within the dates 15–30 July as do the observed. The intensity and phase of the observed water cycle is quite similar to the modeled one.

(c) Let us denote $[\delta W]_{\mathrm{SH}}=[E-P]_{\mathrm{SH}}-[\nabla\cdot Q]_{\mathrm{SH}}$ and $[-\delta W]_{\mathrm{NH}}=[E-P]_{\mathrm{NH}}+[\nabla\cdot Q]_{\mathrm{SH}}$. As revealed from Table 1, the amplitudes of these two quantities and that of $\partial[W]/\partial t$ are comparable, although a slight phase discrepancy exists among them. However, as can be seen in Fig. 9, there is a spring buildup and fall decline of the

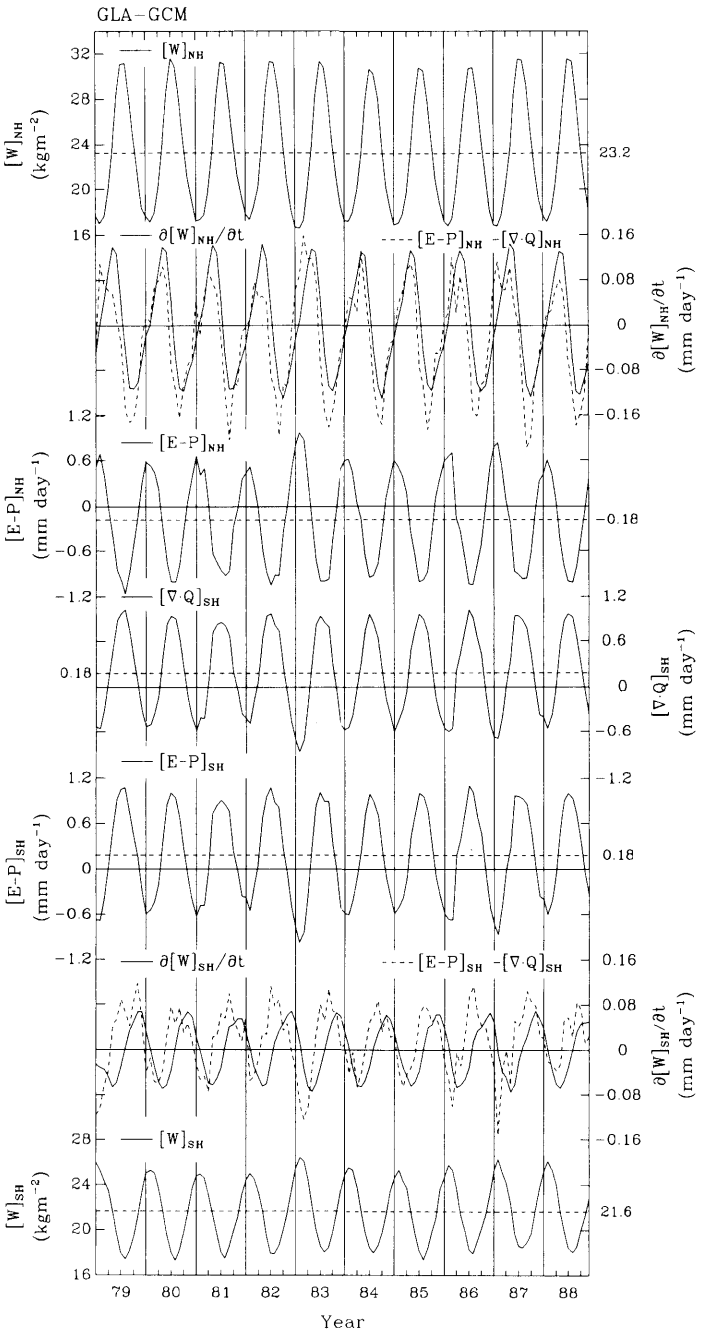

Fig. 9. Same as Fig. 3, except for the hemispheric-mean water budgets simulated by the GLA GCM. Annual variations of $[E-P]_{NH}+[\nabla\cdot Q]_{SH}$ (dashed line) and $[E-P]_{SH}$-$[\nabla\cdot Q]_{SH}$ (dashed line) are also superimposed on those of $\partial[W]_{NH}/\partial t$ and $\partial[W]_{SH}/\partial t$, respectively.

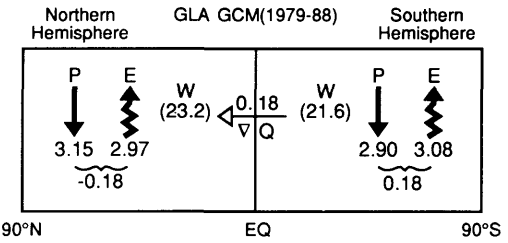

Fig. 10. Same as Fig. 7, except for the hemispheric-mean water budgets simulated by the GLA GCM.

$[W]$ values in both hemispheres. In other words, the annual cycle of the $[\delta W]$ always leads the annual cycle in the $[W]$ by a season.

The fact that the observed and model generated hemispheric water budgets bear a strong resemblance to each other enable us to place some confidence in the simulated climate scenarios.

Let us next examine the time variation in the model's $\langle W \rangle$. Consider the balance equation,

$$\frac{\partial \langle W \rangle}{\partial t} = \frac{1}{2}\{[E-P]_{NH} + [E-P]_{SH}\} = \langle E-P \rangle. \tag{11}$$

The composite annual variations of the model's $-[E-P]_{NH}$ (solid line) and $[E-P]_{SH}$ (dashed line) are shown in Fig. 11. The sum of $1/2\{[E-P]_{NH} + [E-P]\}_{SH} = \langle E-P \rangle$ results in a $\partial \langle W \rangle / \partial t$ which is a season ahead of both of these hydrological variables and $\langle W \rangle$ which is similar to that of the GDAS data, (Fig. 5). The observational $\langle E-P \rangle$ shown in Fig. 5 was inferred from $\partial \langle W \rangle / \partial t$, but annual variations of the model's $\partial \langle W \rangle / \partial t$ and $\langle E-P \rangle$ shown in Fig. 11 are obtained directly from the model diagnostics. After examining Fig. 11, there is little doubt that the annual variation of $\langle W \rangle$ results from that of $\langle E-P \rangle$ as shown in either Fig. 5 or Fig. 11.

The observed $(E-P)$ was computed using a residual method through the vertically integrated water budget equation. Of course, the estimated $(E-P)$ includes errors caused by the data quality and computational errors of the GDAS. However, to reexamine the suggested mechanism by which

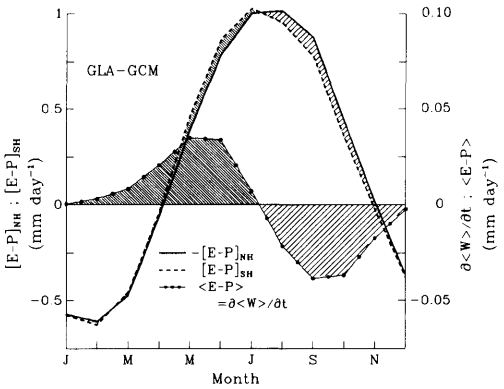

Fig. 11. Same as Fig. 5, except for the hydrological variables simulated by the GLA GCM.

the annual variation of $\langle W \rangle$ is a response of the ocean-atmosphere system to the seasonal march of the overhead sun, composite $\Delta(\chi_Q, Q_D, E-P)$ are produced (Fig. 12b). The dominant wavenumber-1 structure of $\Delta(\chi_Q, Q_D)$, stands out clearly and indicates that in the northern spring more water vapor is converged from the eastern hemisphere and Africa toward the Asian monsoon region and the western Pacific, as was noted with the GDAS data. Moreover, as with the GDAS data, three positive and two negative centers of $\Delta(E-P)$ appear in the tropics. Regardless of any deficiencies in the observational data, the mechanism leading to the $\langle W \rangle$ spring buildup and fall decay suggested in Figs. 6b and 6d is repeated in Fig. 12b which was generated from the hydrological processes as simulated by the GLA GCM. To ascertain the proper simulation of seasonal evolution in hydrological variables by the GLA GCM, the spring-mean $(\chi_Q, Q_D, E-P)$ is also presented in Fig. 12a. The contrast between the observed $\Delta(\chi_Q, Q_D, E-P)$ and $(\chi_Q, Q_D, E-P)$ reappears in Fig. 12.

The major findings related to the observed water budget which were highlighted in the beginning of this section are consistent with the water budget simulated by the GLA GCM. This companion study using simulated data supports our conclusions derived from the observed water budget analysis.

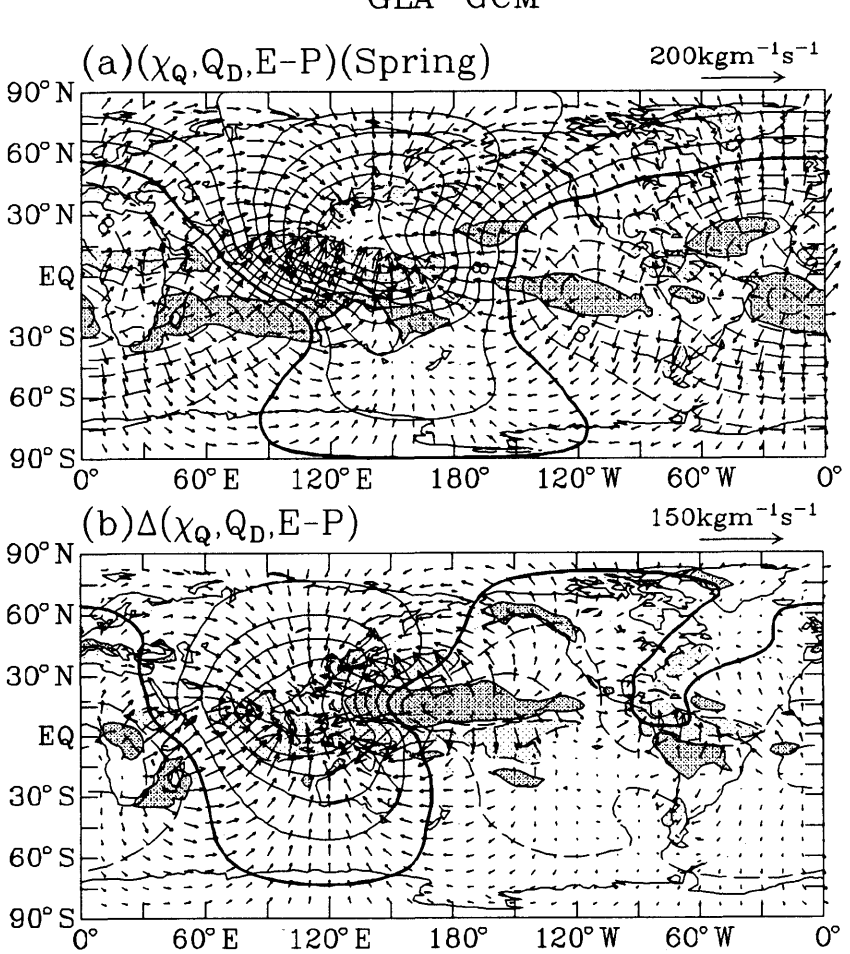

Fig. 12. Same as Fig. 6, except for (a) (χ_Q, Q_D, $E-P$) and (b) $\Delta(\chi_Q, Q_D, E-P)$ simulated by the GLA GCM. χ_Q and $\Delta(\chi_Q)$ are contoured with an interval of 4×10^7 kg m^2 s^{-1} and 2×10^7 kg m^2 s^{-1}, respectively. The positive (negative) values of $(E-P)$ and $\Delta(E-P)$ larger (smaller) than 4 (−4) and 2 (−2) mm day^{-1}, respectively, are heavily (lightly) shaded.

4. Concluding remarks

It was observed that the annual variation of global-mean precipitable water $\langle W\rangle$ follows the annual variation of the Northern Hemisphere mean precipitable water. Although the water vapor transport and budget have been analyzed in numerous earlier studies, the cause of the annual variation in $\langle W\rangle$ was not fully understood. In order to explore the physical mechanism responsible for this annual variation, both the global- and hemispheric ([ ])-mean water budgets were analyzed with the multiyear NMC (1981–1991) and ECMWF (1983–1991) GDAS data, as well as with a 10-year (1979–1988) climate simulation made with a general circulation model of the Goddard Laboratory for Atmospheres. According to the global water budget analysis, the annual variation of global-mean precipitable water $\langle W\rangle$ results from the annual variation of global water

vapor source $\langle E-P \rangle$. In fact, this argument does not shed any light on why the $\langle W \rangle$ annual variations are synchronized with the seasonal march of the Northern Hemisphere. Thus, the hemispheric-mean water budget was pursued.

The hemispheric-mean water budget analysis showed that both the climatological mean and annual variation of $[W]_{NH}$ are larger than those of $[W]_{SH}$. Seasonal marches of the two hemispheres are of opposite phase, but the annual cycle of $\langle W \rangle$ $\{=(1/2)([W]_{NH}+[W]_{SH})\}$ is largely determined by the annual cycle of $[W]_{NH}$. It was shown by previous studies (Bryan and Oort (1984), Chen et al. (1995)) that the Northern (Southern) Hemisphere is a sink (source) hemisphere for water vapor. In other words, precipitable water is climatologically depleted (supplied) from (to) the atmosphere of the Northern (Southern) Hemisphere because $[E-P]_{NH}<0<[E-P]_{SH}$. On the other hand, both $[W]_{NH}$ and $[W]_{SH}$ are climatologically in hydrological equilibrium. In view of these facts, water vapor must be transported across the equator by the Hadley circulation to balance the difference in water budgets between the two hemispheres. The return freshwater flux in the oceans plays the role of balancing this cross-equator atmospheric water vapor transport, as addressed by Chen et al. (1994). At any rate, the cross-equator water vapor transport is a vital factor in determining both the $[W]_{NH}$ and $[W]_{SH}$ annual variations, and in turn the annual variation of $\langle W \rangle$.

Annual variations of $-[E-P]_{NH}$, $[E-P]_{SH}$ and the cross-equator water vapor transport from the Southern to the Northern Hemisphere are synchronized. Based on the hemispheric mean water budget, the annual variation of $[W]_{NH}$ (or $[W]_{SH}$) results from the imbalance between $[E-P]_{NH}$ and $[\nabla \cdot Q]_{SH}$ (or between $[E-P]_{SH}$ and $[\nabla \cdot Q]_{SH}$). This imbalance reaches its maximum and minimum in spring and fall, respectively, and builds up the maximum and minimum values of the $[W]$ values in summer and winter, respectively. However, it can be seen from the differences in the global-scale divergent water vapor transport and water vapor source $(E-P)$ between spring and fall that this spring buildup and fall decline of the $[W]$ values is physically attributable to the east–west differentiation of the atmospheric response over each ocean to the north–south migration of the overhead sun. Thus, this study offers not only the explanation of the $\langle W \rangle$ annual variation, but also a new insight into the global hydrological cycle.

The analysis of the annual variation of the global hydrological cycle undertaken in this study faces some data deficiencies. Specifically, the treatment of initial moisture fields is not subject to any physical constraints in the assimilation systems and the divergent circulation depicted with the assimilated data contains the GDAS biases. The estimation of both $\partial W/\partial t$ and $\nabla \cdot Q$ may be contaminated by these deficiencies in the assimilated data. Consequently, the estimation of $(E-P)$ may also be contaminated by these data deficiencies, in addition to computational errors. For these reasons, the hydrological cycle simulated by a GLA general circulation model was used to compare the water budget obtained with the GDAS data. The observed and simulated global water budgets are quantitatively similar.

Regardless of the new insights into the global water budget gained in this study, some additional studies are urged.

(a) The GLA GCM is not coupled to an oceanic circulation model. The climatological return transport of oceanic freshwater from the Northern to the Southern Hemisphere is missing in the simulated hydrological cycle. Although the parameterizations of surface processes and cumulus convection, together with the prescribed real-time SST, function implicitly as time varying oceans, a natural extension of the present study is to explore the global hydrological cycle simulated by an atmospheric climate model coupled with a full-physics ocean model.

(b) It was pointed out recently by Chen and Pfaendtner (1993) that a synergetic mix of precipitation estimated from spaced-based data and the assimilated data from an operational center's GDAS may offer a better, more consistent delineation of the atmospheric branch of the hydrological cycle. The global precipitation estimated under the Global Precipitation Climatology Project (GPCP) may provide us an opportunity to pursue what was suggested by Chen and Pfaendtner.

(c) The GLA GDAS (Schubert et al., 1993) has been used to generate a 5-year (1985–1989) comprehensively assimilated data set which includes the archiving of precipitation and evaporation in addition to the conventional synoptic

data. Although the hydrological spin-up of the GLA GDAS may impose a model bias on some of the hydrological variables, a complete global hydrological cycle may be obtained from the archived data.

(d) According to the water budget equation, the long-term mean $(E-P)$ is balanced by the divergence of water vapor flux. Because water vapor is a scalar quantity, the divergence of water vapor flux is essentially determined by the divergent circulation. The El Niño-Southern Oscillation (ENSO) activity is the most pronounced interannual variation of the atmospheric circulation. Because the global divergent circulation is an important element of the atmospheric circulation, $\langle W \rangle$ and the global hydrological cycle should also undergo a coherent interannual variation with the ENSO activity. The planned 35-year reanalyzed NMC GDAS data (Kalnay and Jenne, 1991) can be used to explore the interannual variation of the global hydrological cycle.

5. Acknowledgements

This study was supported by the NSF Grant ATM-9345349 and the NASA Grant NAG5-355. We appreciate the typing and editing assistance provided by Mrs. Reatha Diedrichs and Mr. Chris Wikle, respectively. The simulated data were produced with support from the Modeling and Analysis Branch at NASA HQ. Comments offered by two reviewers were helpful in improving the paper.

REFERENCES

Bryan, F. and Oort, A. 1984. Seasonal variation of the global water balance based on climatological data. *J. Geophys. Res.* **89**, 11717–11730.

Chen, T.-C. 1985. Global water vapor flux and maintenance during FGGE. *Mon. Wea. Rev.* **113**, 1801–1819.

Chen, T.-C. and Tzeng, R.-Y. 1990. Global-scale intraseasonal and annual variation of divergent water-vapor flux. *Meteorol. Atmos. Phys.* **44**, 133–151.

Chen, T.-C. and Yen, M.-C. 1991. A study of the diabatic heating associated with the Madden-Julian Oscillation. *J. Geophys. Res.* **96**, 13163–13177.

Chen, T.-C. and Pfaendtner, J. 1993. On the atmospheric branch of the hydrological cycle. *J. Climate* **6**, 161–167.

Chen, T.-C., Pfaendtner, J. and Weng, S.-P. 1994. Aspects of the hydrological cycle of the ocean-atmosphere system. *J. Phys. Oceanogr.* **24**, 1827–1833.

Chen, T.-C., Chen, J.-M. and Pfaendtner, J. 1995. Low-frequency variations in the atmospheric branch of the global hydrological cycle. *J. Climate* **8**, 92–107.

Kalnay, E. and Jenne, R. 1991. Summary of the NMC/NCAR reanalysis workshop of April 1991. *Bull. Amer. Meteor. Soc.* **72**, 1897–1904.

NOAA Global Precipitation Program Science Team, 1991. Global Precipitation Science Plan for the NOAA Climate and Global Change Program, University Corporation for Atmospheric Research, NOAA Climate and Global Change Program. *Special Report, no.* **6**, pp. 15.

Oort, A. H. 1971. The observed annual cycle in the meridional transport of atmospheric energy. *J. Atmos. Sci.* **289**, 325–339.

Peixoto, J. P. and Oort, A. H. 1983. The atmospheric branch of the hydrological cycle and climate. *Variations of the global water budget* (ISBN 90-277-1364-2), Reidel, London, 5–65.

Rosen, R. D., Salstein, D. A. and Peixoto, J. P. 1979. Variability in the annual fields of large-scale atmospheric water vapor transport. *Mon. Wea. Rev.* **107**, 26–37.

Schubert, S. D., Rood, R. B. and Pfaendtner, J. 1993. An assimilated data set for earth science application. *Bull. Amer. Meteor. Soc.* **74**, 2331–2342.

Stephens, G. L. 1990. On the relationship between water vapor over the oceans and sea surface temperature. *J. Climate* **3**, 634–645.

Sud, Y. C. and Walker, G. K. 1993. A rain evaporation and downdraft parameterization to complement a cumulus updraft scheme and its evaluation using GATE data. *Mon. Wea. Rev.* **121**, 3019–3039.

Trenberth, K. E., Christy, J. R. and Olsen, J. G. 1987. Global atmospheric mass, surface pressure, and water vapor variations. *J. Geophys. Res.* **92**, 14815–14826.